ELSEVIER

0144-8617(94)00051-4

Carbohydrate Polymers 25 (1994) 187–195

0144-8617/94 $07.00

Static light scattering technique applied to pectin in dilute solution. Part II: The effects of clarification

Gisela Berth,[a]*† Herbert Dautzenberg[b] & Gudrun Rother[b]

[a]*Deutsches Institut für Ernährungsforschung Potsdam-Rehbrücke, Arthur-Scheunert-Allee 114–116, D-14558 Bergholz-Rehbrücke, Germany*
[b]*Max-Planck-Institut für Kolloid- und Grenzflächenforschung, Kanstr. 55, D-14513 Teltow-Seehof, Germany*

(Received 22 June 1993; accepted 7 February 1994)

The effects of purification/clarification by ultracentrifugation and/or membrane filtration were studied by light scattering, GPC plus off-line capillary viscometry and GLC sugar analysis using a high-methoxyl citrus pectin as model substance. The emphasis of light scattering measurements was put on analysing the angular dependence of the scattered light. For that reason the interpretation of the measured data involved the use of master curves in addition to Zimm or Guinier plots. The benefits and limitations of this method of data treatment for complex systems are discussed both in theory and practice.

Due to the natural heterogeneity of pectins, purification or classification modified the original sample by removing the high molecular weight and dense tail, leaving a physically and chemically heterogeneous polysaccharide.

INTRODUCTION

The application of static light scattering to a concentration series of commercial pectins has revealed that the data obtained are very sensitive to the conditions chosen for clarification (Part I of this series). This suggested more basic studies of the effect of the purification process (membrane filtration and ultracentrifugation) using a more sophisticated interpretation of light scattering data by means of master curves (Dautzenberg & Rother, 1988, 1992). The method was developed in particular for the interpretation of strongly curved scattering curves that result from large particles. In this case neither the Zimm procedure (Zimm, 1948) nor the Guinier plots (Kerker, 1969) is appropriate and does not allow correct extrapolation to zero angle. The master curve interpretation works by comparing the measured scattering curve with theoretically calculated curves. The latter are obtained for different structural models such as spheres of homogeneous density and Gaussian coils, respectively, having different polydispersities. From a fitting of the experimental curve with one out of a set of theoretical curves one can draw conclusions about the structure size, polydispersity and polymer density within the particles. This paper is concluded with some results of glycoside analysis by GLC and gel-permeation chromatography (GPC) plus viscometry.

*To whom correspondence should be addressed.
†Present address: Institute of Biotechnology, University of Trondheim, N-7034 Trondheim, Norway.

EXPERIMENTAL

Details of the pectin sample used, membrane filtration and light scattering technique are described elsewhere (Part I of this series).

Ultracentrifugation was carried out in a preparative ultracentrifuge type VAC 602 (MLW, Germany) at 50 000 rpm for 4 h. Supernatants were carefully isolated from the precipitate by means of a syringe.

Samples of the air-dried precipitate and the lyophilized supernatant were taken for the glycoside analysis by GLC after hydrolysis in trifluoroacetic acid or sulphuric acid. Galacturonic acid was determined colorimetrically (Kravtchenko *et al.*, 1992).

GPC on Sepharose Cl-2B/Sepharose Cl-4B, the determination of the E_q values, and viscosity measurements were described previously (Berth, 1988).

DATA ANALYSIS

From the fluctuation theory (e.g. Tanford, 1965) one obtains for the Rayleigh ratio of the scattering intensity of a monodisperse solution the simple expression:

$$\frac{K \cdot c}{R_\theta} = P^{-1}(\theta)\left[\frac{1}{M} + 2Bc + 3Cc^2 + \dots\right], \qquad (1)$$

where the Rayleigh ratio is defined by $R_\theta = I_\theta/(I_0 \times r^2)$, I_θ = net scattering intensity relative to the solvent measured at the scattering angle θ, I_0 = intensity of the primary beam, r = distance between the scattering volume and the observer, K is a constant factor which contains the optical parameters of the system, c = mass concentration of the polymer in g ml^{-1}, $P(\theta)$ = intraparticular scattering function, M = molecular mass, and B and C are second and third virial coefficients. For polydisperse systems, light scattering yields the weight average value of the molecular mass M_w and the z-average of the intraparticular scattering function $P_z(\theta)$ of the scattering species. Describing the polydispersity by a normalized mass distribution function $p_w(M)$ these quantities are defined by

$$M_w = \int_0^\infty M p_w(M)\,\mathrm{d}M \qquad (2)$$

$$P_z(\theta) = \frac{1}{M_w}\int_0^\infty M P(\theta, M) p_w(M)\,\mathrm{d}M. \qquad (3)$$

In the framework of the Rayleigh–Debye approximation, which describes the angular dependence in terms of a pure interference effect between the scattered light from different centres of the scattering particle:

$$P(q) = \frac{1}{N_s^2}\sum_{i,j}\frac{\sin q \cdot r_{ij}}{q \cdot r_{ij}}, \qquad (4)$$

where N_s = number of scattering centres in the particle, r_{ij} = distance between the scattering centres i and j, $q = 4\pi/\lambda \sin\theta/2$, and λ = wavelength in the medium. By a series expansion of the sine term it follows from eqns (3) and (4) that, whatever the shape and internal structure of the scattering particles is,

$$P_z(q) = 1 - \tfrac{1}{3}\langle s^2\rangle_z q^2 + \dots, \qquad (5)$$

where $\langle s^2\rangle_z$ is the z-average of the square of the radius of gyration. Introducing eqn (5) into eqn (1) gives the well-known formula commonly used in analysing light scattering experiments on polymer solutions:

$$\frac{k \cdot c}{R_\theta} = \frac{1}{M_w} + \frac{16\pi^2\langle s^2\rangle_z}{3\lambda^2 M_w}\sin^2\frac{\theta}{2} + 2Bc + \dots \qquad (6)$$

Normally, data are plotted as a Zimm plot (Zimm, 1948) in which $k \cdot c/R_\theta$ is plotted against $\sin^2\theta/2 + k \cdot c$, where k is arbitrarily chosen in order to attain an appropriate spreading of the data (see Huglin, 1972, and Part I of this series). The extrapolations to zero concentration and zero angle yield values of M_w from the intercept on the ordinate as well as B and $\langle s^2\rangle_z$ from the slopes of the extrapolated curves. For coil-like structures of flexible polymers this procedure works well. The situation changes drastically for large (>100 nm) and more compact particles. The scattering curves then become strongly curved, particularly in the small angle range, and the extrapolations in a Zimm plot may show large uncertainties. On the other hand, scattering curves of such systems contain more structural information because the scattering function is known at a higher range of the argument and reflects the structure type and the polydispersity of the scattering system. An assessment of these structural details as well as a reliable determination of the mass and size of the scattering particles may be achieved by a data analysis which is based on a comparison of the experimental scattering curves with theoretical ones which are calculated for various basic structural types (Dautzenberg & Rother, 1988, 1992). The intraparticular scattering functions $P(\theta)$ are known for a great variety of structures (see, e.g. Kerker, 1969). Using these expressions and assuming a distribution function for the molecular mass, $P_z(\theta)$ can be calculated according to eqn (3).

However, even for monomodal distributions such as the Schulz–Zimm or the logarithmic distribution (cf. Part I of this series) $P_z(q)$ depends on two parameters (size and polydispersity). Fortunately, in the Rayleigh–Debye approximation the intraparticular scattering functions depend on the product of q and the size parameter. Therefore, in a double logarithmic plot the change of the size parameter corresponds only to a shift along the abscissa and the size dependence of $P_z(q)$ may be represented by a single curve. One then obtains for a given structure type a set of scattering curves for different polydispersities. As was shown by Dautzenberg & Rother (1992) the choice of a particular distribution function has no essential influence on the shape of the scattering curves so that the structural type, and, for compact particles, the polydispersity can be clearly assessed if the experimental scattering function is known in a sufficiently large angular range. Since the experimentally available quantity $R_\theta/k \cdot c$ is proportional to M_w one can compare these curves directly with the theoretical ones in the double logarithmic plot because a change of M_w corresponds only to a shift of the curve along the ordinate. Having fitted the experimental curve with a section of an appropriate theoretical curve one obtains directly the size parameter and the value of M_w from the position of the experimental curve relative to the theoretical one.

However, it must be stressed that the application of this kind of data interpretation is justified only for highly diluted systems where the virial terms can be neglected or, in the case of data, extrapolated to zero concentration. Moreover, one must be aware that the

interpretation is not unique because, as in the case of spheres, a deviation from the spherical shape, or an internal density gradient would correspond to an additional polydispersity.

Since, in the double logarithmic plot the shape of the scattering function does not depend on M_w, and the size parameter 'shifts' the experimental curve only along the model curve, this procedure is called a 'scaled representation' or 'interpretation by master curves'.

The master curve interpretation of experimental scattering curves is also helpful in correctly analysing data obtained on bimodal systems consisting of a compact particulate and a molecularly dissolved component. The precondition for doing so is that the contributions of both components are pronounced in the scattering curve. Due to the strong angular dependence of their scattering curves, large particles dominate the scattering behaviour within the small angle region. As a first step, their structural parameters can be estimated by the master curve interpretation and then their scattering contribution can be separated from the measured curve. The remaining curve should then be analysed by means of a Zimm plot, giving a first approximation to the parameters of the molecularly dispersed component so that its contribution can be subtracted from the original curve. As an iterative procedure it leads to reliable information on both components.

RESULTS AND DISCUSSION

Figure 1(a) illustrates the effects of the two most common clarification procedures on the size distribution curves measured by GPC. Centrifugation removes about 10% of the original sample and filtration through a 0·2 μm pore size membrane filter removes approximately 15%. Compared with the original material purification has particularly reduced components with large hydrodynamic volumes which are eluted close to the void volume of GPC. The higher intrinsic viscosities found for the supernatant after ultracentrifugation (Fig. 1(b)) indicate unambiguously the preferred loss of particulate matter. This is in good agreement with previous results (Berth, 1988; Berth *et al.*, 1990; Berth & Lexow, 1991) where we have identified compact structures rich in neutral sugar components which are present in the first stages of polysaccharide elution. The extinction quotients E_q also given in Fig. 1(a) were derived from UV spectra after addition of highly concentrated sulphuric acid. E_q increases after purification, showing that the galacturonic acid to neutral sugar ratio increases although, as before, neutral sugars remain distributed along the elution volume axis in a characteristic manner (Berth & Lexow, 1991).

The sugar analysis by GLC (Table 1) reveals all the neutral sugars, typically present in fruit pectins, both in the supernatant and the macroscopically inhomogeneous precipitate. Although the sum of both does not correspond perfectly to the original in the first column, this result classifies the precipitated carbohydrate as pectin—either covalently bound to or mixed with celluloses/hemicelluloses. The high rhamnose content suggests the enrichment of 'hairy regions' released by β-elimination (Berth *et al.*, 1990). Table 1 provides considerable support for relating all concentration data to the total carbohydrate; contrary to the often used

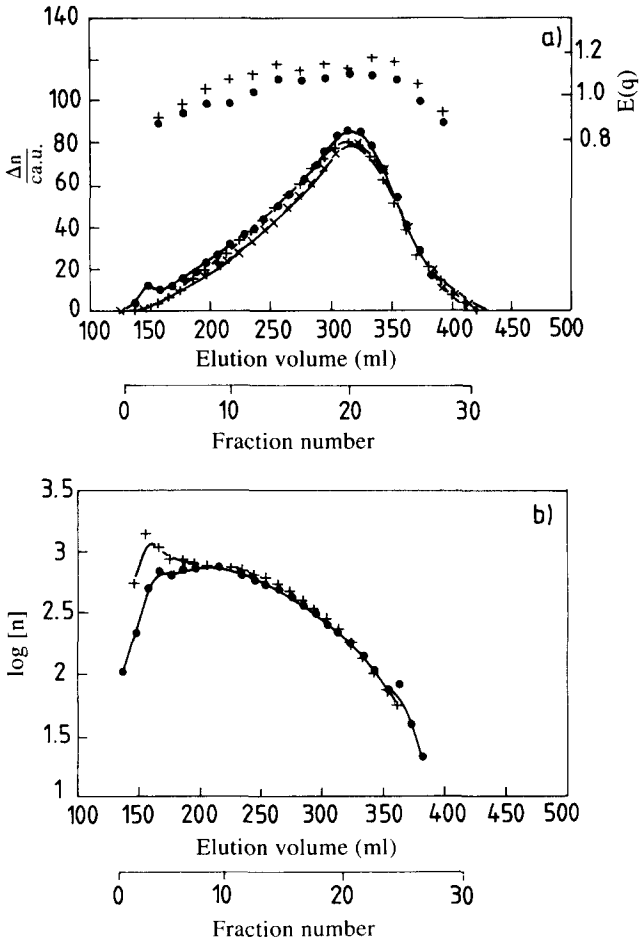

Fig. 1. Elution lines on Sepharose Cl-2B/Sepharose Cl-4B: (a) E_q values, and (b) intrinsic viscosities of the fractions. ●, original; +, supernatant of ultracentrifugation; ×, filtrate (0·2 μm pore size, three times).

Table 1. Citrus pectin from Koch-Light—glycoside composition (mol%)

Glycoside	Original	Supernatant	Precipitate[a]
GalA	88·32	89·19	63·90
Rha	1·68	1·49	9·30
Ara	4·79	4·56	4·88
Gal	4·41	4·26	5·50
Glc	0·60	0·32	14·35[b]
Xyl	0·16	0·16	0·45
Man	0·09	0·07	1·64

[a]About 10% of the original.
[b]No starch—hemicellulose?/cellulose?

practice of considering only the galacturonic acid content. The latter method ignores the copolymeric nature of pectins, which is of decisive influence on their physicochemical and functional properties (Berth & Dahme, 1991). The optical properties of the different monomers are significantly similar, allowing pectins to be treated as homopolymeric polyelectrolytes from the viewpoint of light scattering and concentration determinations via refractive index measurements.

Consequently, we used a calibrated differential refractometer for determining the recovery rates when we 'clarified' a solution containing initially 5 mg ml^{-1} of the air-dried original substance by ultracentrifugation and/or successive filtration through membrane filters of decreasing pore size. ('Successive filtration' means filtering the solution through a 5·0 μm pore size filter at first followed by filtration through 1·2 μm pore size filters and so on.) Results are given in Table 2 and 3.

The corresponding light scattering data are collected in Figs 2 and 3. The same data are presented as Zimm, Guinier and master plots. The Zimm plot of the original solution after successive filtration through pore sizes from 5·0 down to 0·2 μm shows a set of slightly upward curved lines (Fig. 2(a)). While the common procedure of extrapolation to zero angle leads to $M_w \sim 11{\cdot}7$ million for curve 4 (0·45 μm), the three lower curves are hardly expected to give accurate molecular parameters since even small uncertainties in the extrapolation are associated with vastly different results. The Guinier plot (Fig. 2(b)) reveals the strongest curvature and the highest scattering level for the largest pore size filtrate and systematically reduced values for the smaller pore size filtrate. This indicates, together with the first column in Table 2, the progressive loss of small amounts of the largest species.

Unfortunately, the extrapolation of the curved small angle region data in Fig. 2(b) involves large uncertainties with respect to the absolute intensity and the initial slope also. That is why we applied the interpretation of the measured data by means of master curves (Fig. 2(c)). All experimental curves (crosses) could be fitted perfectly with theoretical curves for spheres of homogeneous density. Results are listed in Table 2. It shows the decreasing M_w and a_m as well as $\langle s^2\rangle_z^{1/2}$ values for the remaining percentages of the solute according to the first column. The decreasing polymer densities ρ suggest the preferred removal of more dense particles. A loss of 12% in matter between 5·0 and 0·2 μm pore size (column 1) is accompanied with a reduction to almost one-fifth of the initial value (column 6).

In order to assess better the process of filtration it might be worthwhile to consider the molecular characteristics of the retained matter. This is not directly available, but can be obtained from the difference of the scattering curves related to the actual mass contribution from Table 2. Consequently, we have subtracted the curves in question (Fig. 2)—this means '5·0–1·2 μm, '1·2–0·8 μm', etc.—and obtained Fig. 4. The loss in material was taken into account by introducing a factor $q(q < 1)$ on the basis of the data in Table 2 (first column) for the scattering curve to be subtracted. The

Table 2. Results of filtration on the original pectin sample solution in phosphate buffer, pH 6·5 (c_0 = 5 mg ml^{-1})

Recovery related to the air-dried original (%, w/w)	Pore size of membrane filter (μm)	Results of master curve interpretation from Fig. 2 (model: spheres of homogenous density)				
		δ_a	a_m (nm)	M_w / $x_2 M_{w_2}$	ρ (g ml^{-1}) / $x_2\rho_2$	$\langle s^2\rangle_z^{1/2}$ (nm)
91·25	Unfiltered					
90·50	5·00	0·600	186	$1{\cdot}673\times10^{8}$	$1{\cdot}023\times10^{2}$	356
90·25	1·20	0·600	162	$8{\cdot}983\times10^{7}$	$7{\cdot}396\times10^{3}$	309
89·60	0·80	0·600	148	$5{\cdot}175\times10^{7}$	$6{\cdot}371\times10^{3}$	281
86·50	0·45	0·600	107	$1{\cdot}160\times10^{7}$	$3{\cdot}739\times10^{3}$	205
80·50	0·20	0·600	68	$1{\cdot}793\times10^{6}$	$2{\cdot}243\times10^{3}$	130

Table 3. Results of filtration on the ultracentrifuged pectin solution in phosphate buffer, pH 6·5 (c_0 = 5 mg ml^{-1})

Recovery related to the air-dried original (%, w/w)	Pore size of membrane filter (μm)	Structure features	M_w (extrapolated from Zimm plot)	Results of master curve interpresentation
84·80	Unfiltered			
83·00	5·00	Bimodal spheres	n.d.	$\delta_a = 0{\cdot}6, a_m = 66$ nm, $x_2 M_{w_2} = 3{\cdot}411\times10^{5}$
80·00	1·20	Bimodal spheres	n.d.	
79·50	0·80	Bimodal spheres	n.d.	$\delta_a = 0{\cdot}6, a_m = 302$ nm, $x_2 M_{w_2} = 4{\cdot}002\times10^{6}$
74·00	0·45	Bimodal spheres	100 000	
59·00	0·20	Bimodal spheres	36 000	

n.d. = not determined.

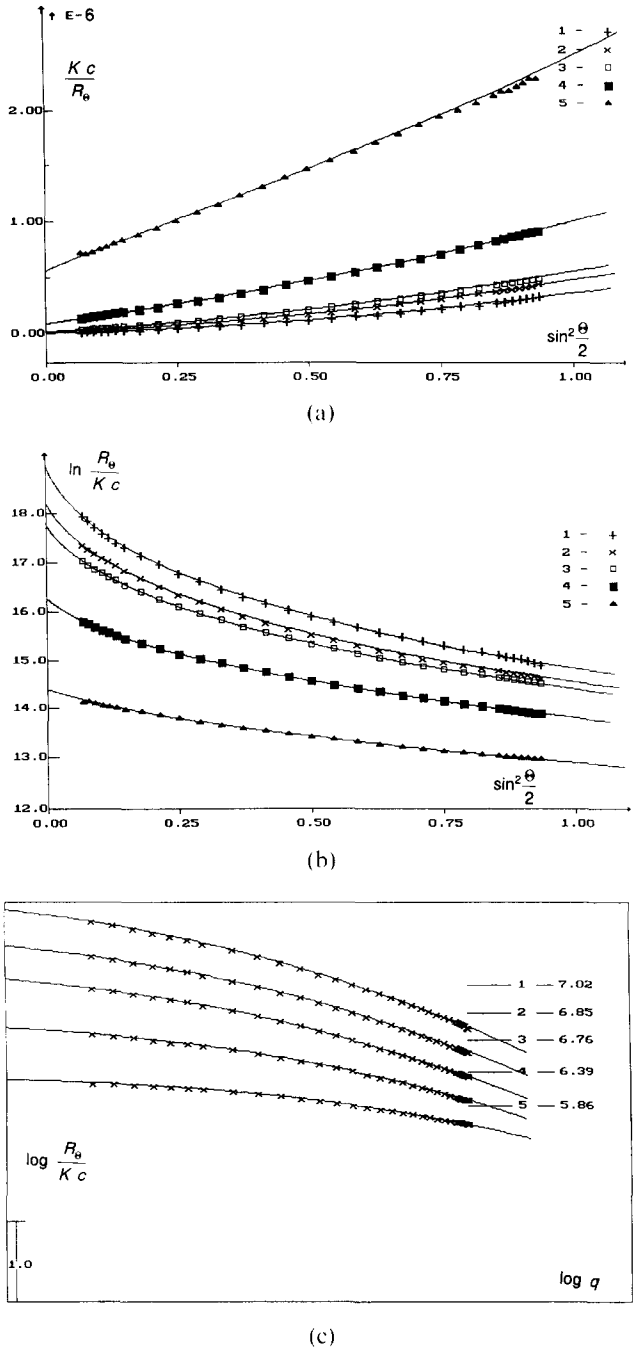

Fig. 2. Light scattering data obtained for citrus pectin in phosphate buffer after filtration through membrane filters of successively diminished pore size (3× each); 1, 5·0 μm; 2, 1·2 μm; 3, 0·8 μm; 4, 0·45 μm; 5, 0·2 μm. (a) Zimm plot; (b) Guinier plot; (c) master plot.

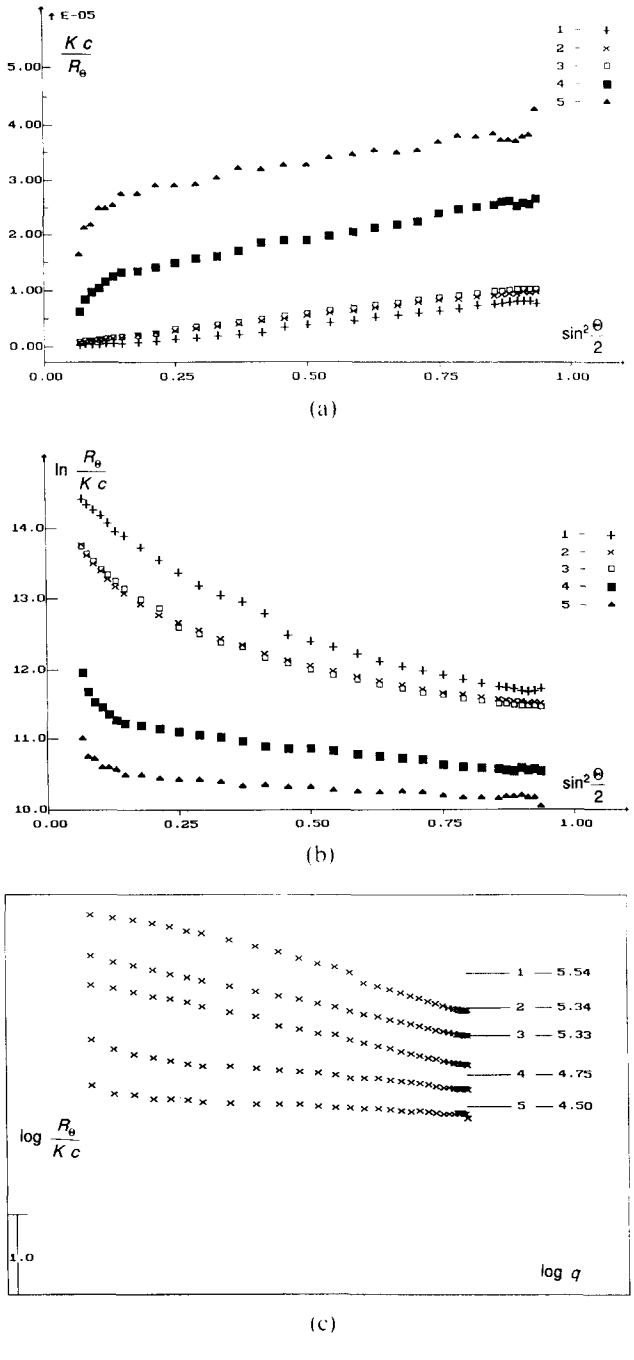

Fig. 3. Light scattering data obtained for citrus pectin in phosphate buffer after ultracentrifugation and filtration through (for further details see Fig. 2).

resulting master curves could also be interpreted in terms of a monomodal system of polydisperse spheres of homogeneous density. Results in Table 4 indicate filtration through 5·0 and 1·2 μm retains the extremely dense and high molecular weight species (possibly cell wall debris) while the subsequent filtration steps remove also smaller and increasingly better solvated species of the population.

These findings require a more basic consideration. Obviously we are *always* faced with a smaller amount of a particulate matter containing system. Such systems are difficult to handle (e.g. Kratochvil, 1972). Their light scattering behaviour is dominated by the large particles of mass fraction x_2 (cf. Part I of this series), whereas the concentration terms of the Rayleigh–Debye formula normally consider the total polymer concentration c. Under these circumstances the resulting weight average molecular weight represents an average

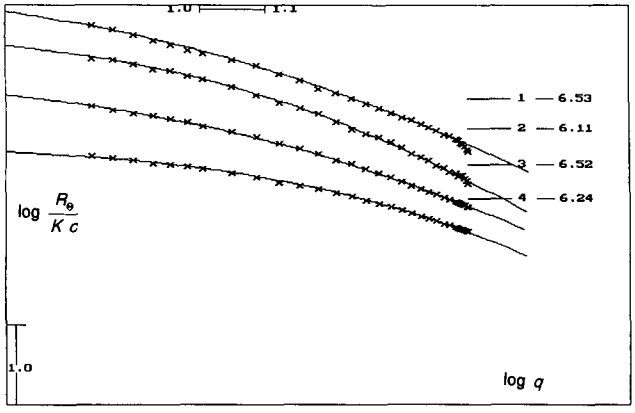

Fig. 4. Calculated master curves for the retained by filters proportion from Fig. 2 and Table 2: 1, 5·0–1·2 μm; 2, 1·2–0·8 μm; 3, 0·8–0·45 μm; 4, 0·45–0·2 μm.

value over rather different species with little in common. Therefore, the average value need not have any physical meaning. Systems of that nature are more adequately represented when they are interpreted on the basis of a bimodal distribution according to $M_w = x_1 M_{w_1} + x_2 M_{w_2}$ where the index '1' denotes the molecularly dispersed proportion and $x_1 + x_2 = 1$. As long as $x_1 M_{w_1} \ll x_2 M_{w_2}$ we can neglect the contribution of the molecularly disperse proportion and assign the experimentally found intensities to $x_2 M_{w_2}$ (although $x_1 \gg x_2$). This is the case for pore sizes of 0·8 μm and over with certainty, and M_w as well as ρ should be replaced by $x_2 M_{w_2}$ and $x_2 \rho_2$, respectively. Assuming $x_2 = 0{\cdot}01$, M_{w_2} increases by two orders of magnitude, approaching values which were obtained definitely (Table 4). Consequently, systems are extremely sensitive to all changes in $x_2 M_{w_2}$, while the other term forms only the weakly scattering background. Changes concerning this proportion can hardly be observed. There is no reason for assuming the filtration yields physically homogeneous pectin solutions. The effect of filtration consists of narrowing the distribution of the particulate matter and hence the distribution of the whole pectin sample.

Considering analogously the effect of filtration on solutions pretreated by ultracentrifugation (Table 3 and Fig. 3) we are faced with a lower initial recovery rate and—what requires particular emphasis—a significantly increased loss after filtration through 0·2 μm pore size. It looks as if the centrifugation step has generated much larger aggregates. In contrast to the original solution the reduction in pore size from 1·2 to 0·8 μm has no additional effect.

Once again we present the Zimm, Guinier and master plots for the same experimental data. Curves 1–3, corresponding to filtration through 5·0, 1·2 and 0·8 μm pore size filters show strongly curved Guinier and master plots, which is indicative of large spheres alone or as a mixture. An experienced observer will realize a slight trend towards bimodal distributions when comparing Fig. 3 with Fig. 2. For reasons discussed in Part I of this series the same data leads to flat and almost straight lines when plotted according to Zimm. The bimodal character is much more developed after filtration through 0·45 and 0·2 μm pore size membranes. The presence of tiny amounts of high molecular weight particulate matter causes a downward curvature within the small angle region below 40° of the Zimm plot (see Part I) and correspondingly an upward curvature in the Guinier and master plots. This is because the scattering contribution of the particles is large at small angles, but becomes small in the wide angle region compared with the contribution of the molecularly dispersed major fraction. Evidently, filtration even when combined with ultracentrifugation cannot yield absolutely particle-free solutions. However, the ultracentrifugation brought an additional loss in polysaccharide matter together with an overproportional reduction of the scattering level (compare Figs 2(b) and 3(b)).

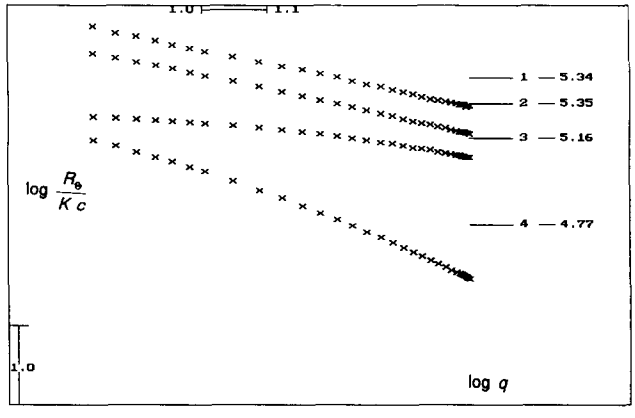

Fig. 5. Scattering curve separation by means of master curves for curve 2 from Fig. 3. 1, measured curve; 2, sum of the model curves 3 and 4; 3, model curve for spheres $\delta_a = 0{\cdot}600$, $a_m = 66$ nm, $M_w = 3{\cdot}411 \times 10^5$; 4, model curve for spheres $\delta_a = 0{\cdot}600$, $a_m = 302$ nm, $M_w = 4{\cdot}002 \times 10^6$.

Table 4. Results of the master curve interpretation of the difference scattering curves according to Fig. 4 and Table 2 (molecular parameters of the particulate matter retained by filtration)

Pore size (μm)	δ_a	a_m (nm)	M	ρ (g ml^{-1})	$\langle s^2 \rangle_z^{1/2}$ (nm)
5.00–1.20	0.600	224	3.461E+10	1.225	426
1.20–0.80	0.450	201	1.564E+9	0.077	258
0.80–0.45	0.600	177	1.643E+9	0.095	338
0.45–0.20	0.450	122	1.172E+8	0.025	157

The quantitative interpretation of the scattering curves in Fig. 3 is difficult and requires some experience. Using the master plot technique we could fit the experimentally obtained curve 2 from Fig. 3(c) by the sum of model curves of homogeneous spheres having $\delta_a = 0{\cdot}6$ and $a_m = 66$ nm and $a_m = 302$ nm, respectively. Figure 5 shows the single steps of curve separation where curves 3 and 4 stand for the individual models. Curve 2 is the calculated sum of both, which shows best agreement with the experimental curve 1. This result suggests that even the particulate matter is not a homogeneous fraction. All the discussions above concerning the role of the molecularly dispersed proportion and the meaning of the average parameters such as molecular weight and density are valid as well. A somewhat simpler interpretation can be made in the case of curves 4 and 5 in Fig. 3 when the contribution of the particle component almost disappears for wide angles, and the scattering contribution of the molecularly dispersed fraction dominates. Neglecting the small angle curvature and extrapolating linearly the wide angle region data to zero angle (Fig. 3(a) or (b)) one obtains an M_w of about 36 000 for the 0·2 μm and $M_w \sim 100\,000$ for the 0·45 μm pore size filtrate, respectively. It cannot be stressed enough that these values hold when almost 36 or 19% of the original polysaccharide was discarded. As they are obtained at finite concentration they must not be directly compared with previously reported sedimentation results (Harding *et al.*, 1991*a*). In order to compensate for the concentration effect a B value of $2{\cdot}8\times10^{-2}$ ml mol g^{-2} (for $M_w \sim 36\,000$ at $c = 2{\cdot}94$E-3 g ml^{-1}) is required, which seems unrealistic (Harding *et al.*, 1991*b*). It is more likely that filtration through 0·2 μm has already removed part of the molecularly dispersed pectin fraction (see also Berth *et al.*, 1990).

For reason of completeness we have also obtained the difference curves for the ultracentrifuge supernatant after filtration. The complex character of the resulting scattering curves (not shown) restricted their interpretation. All the results discussed so far reflect the complexity of the subject and show that there is no simple experimental approach to the problem. Our work emphasizes a widespread problem in polysaccharide analysis, particularly when studies are performed by high-performance size exclusion chromatography (HPSEC). The use of HPSEC columns requires the injection of exhaustingly prepurified solutions, otherwise the columns can easily be blocked. This often means excluding considerable amounts of the original substance prior to loading.

In a previous paper (Berth, 1992) we have shown that GPC can fail to separate particulate matter from the molecularly dispersed component. Having fractionated the unpurified sample and used a membrane filter of 0·45 μm pore size to clarify the fractions prior to off-line light scattering measurements we developed an algorithm for the interpretation of the scattering curves

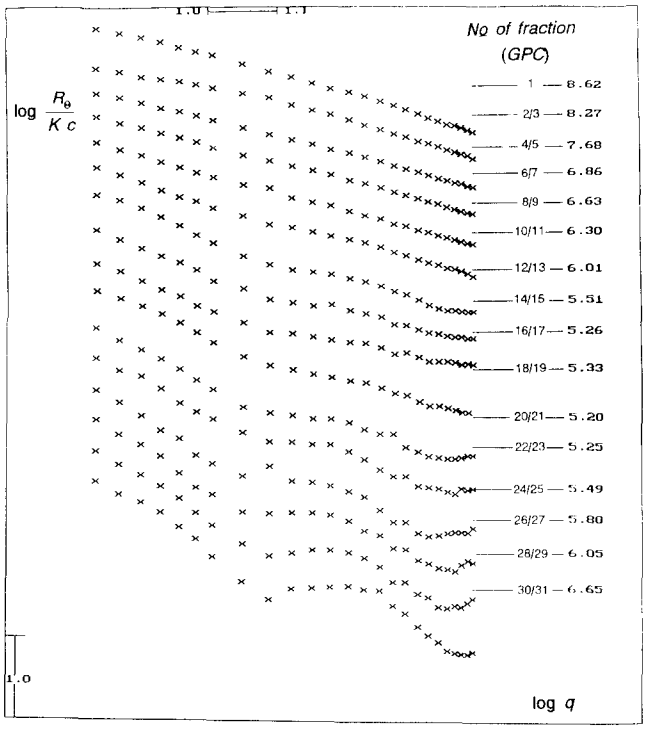

Fig. 6. Master curves obtained for the GPC fractions according to Fig. 1 for the unpurified pectin after filtration through one 5·0 μm pore size membrane filter.

in terms of a two-component system (Berth *et al.*, 1990). The molecular weights found for the particle-free proportion were in excellent agreement with the results of ultracentrifugation on comparable GPC fractions (Harding *et al.*, 1991*a*). When the same procedure was applied using a 5·0 μm pore size membrane we obtained the master curves given in Fig. 6 (see the GPC elution line in Fig. 1 also). They show the gradual transition from initially broadly distributed polydisperse systems of homogeneous spheres (fractions 1, 2/3) to bimodal systems of narrowly distributed spheres with increasing elution volume/number of fraction. The first two curves could still be interpreted monomodally with $\delta_a = 0{\cdot}8$ and 0·6 and a_m values of 254 and 158 nm, respectively. The scattering curve for fractions 18/19 for the GPC peak maximum (Fig. 1) was analysed analogously to Fig. 5 and gave the results shown in Fig. 7. From that it can be seen that the experimental curve was adequately represented by the theoretical curve of a mixture of spheres having radii a_m of 109 and 360 nm and polydispersities of 0·2 and 0·15. As the entire angular range is determined by the large spheres one cannot obtain any information on the molecularly dispersed proportion.

The increasing average radii of gyration, especially for the later stages of elution, together with an average molecular weight minimum along the elution volume axis (at fraction 20/21 of Fig. 1), indicate all but an ideal behavior. The bimodal distribution even for the parti-

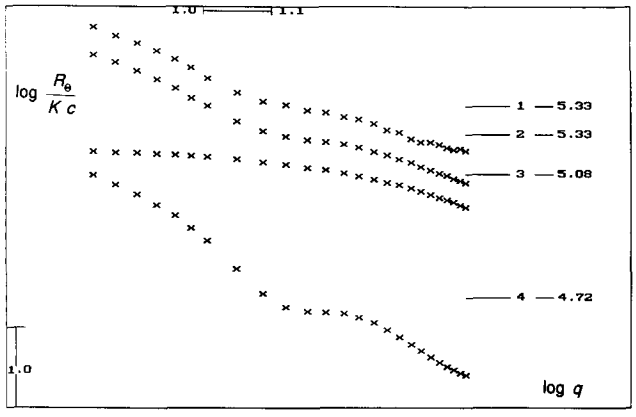

Fig. 7. Scattering curve separation by means of master curves for the GPC fraction 18/19 from Figs 1 and 6. 1, measured curve; 2, sum of the model curves 3 and 4; 3, model curve for spheres $\delta_a = 0{\cdot}200$, $a_m = 109$ nm, $M_w = 2{\cdot}76 \times 10^5$; 4, model curve for spheres $\delta_a = 0{\cdot}150$, $a_m = 360$ nm, $M_w = 7{\cdot}62 \times 10^6$.

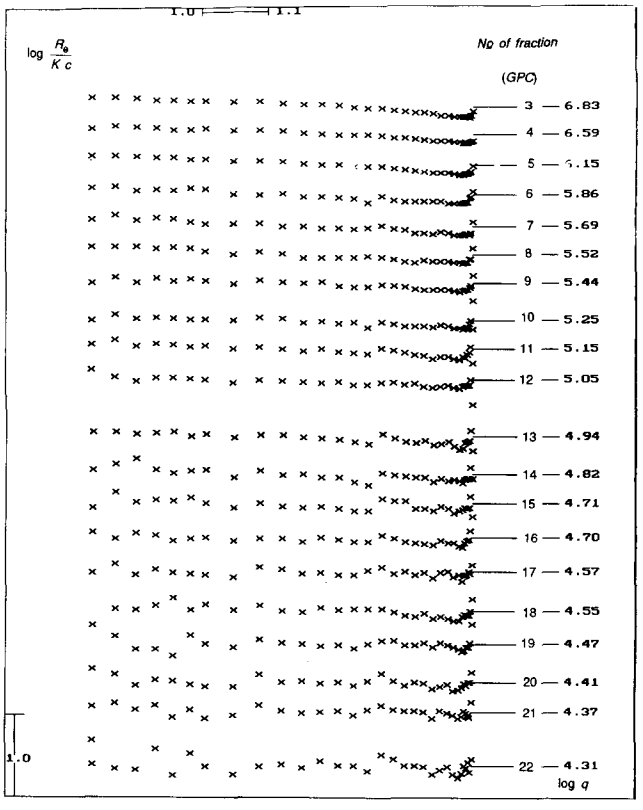

Fig. 8. Master curves obtained for the GPC fractions according to Fig. 1 for the sharply filtered prior to loading pectin solution.

culate matter are consistent with the results from β-elimination on the same pectin (Berth *et al.*, 1990) and data obtained by GPC plus light scattering on 'modified hairy regions' isolated from apple juice (Berth, unpublished; sample preparation: Schols, H., Agricultural University of Wageningen, The Netherlands). It cannot be denied that 'hairy regions' due to their compact structure explain the occurrence of the particulate matter in pectins.

The GPC line in Fig. 1, together with the master curve collection in Fig. 8, reveals the effect of the exhausting prepurification by filtration prior to loading the GPC columns as is usual practice in HPSEC studies. The pectin solution was filtered through a filter series from 5·0 down to 0·2 μm pore size three times. To clarify the eluent we used a pore size of 0·45 μm. Master curves obtained under these conditions are flat and show the normal decrease in molecular weights with the elution volume—an almost ideal behaviour. The scattering curves can be fitted by model curves of Gaussian coils as well as small spheres (Dautzenberg & Rother, 1988). This is consistent with the fact that light scattering gives no reliable information on the shape of scatterers when there is only a slight angular dependence. In this case another way of data plotting (Guinier or Zimm) is appropriate, as is shown in Fig. 9.

Consequently, all 'distortions' at GPC and problems with light scattering data interpretation arise from the natural heterogeneity of pectins and can only be partly overcome by a rigorous 'prepurification' which modifies the original sample. The remaining slight angular dependence, however, does not justify the conclusion that the sample obtained is chemically and physically homogeneous. To check homogeneity, additional studies are required.

Even after previous studies by GPC combined with light scattering and viscometry we had to drop the idea

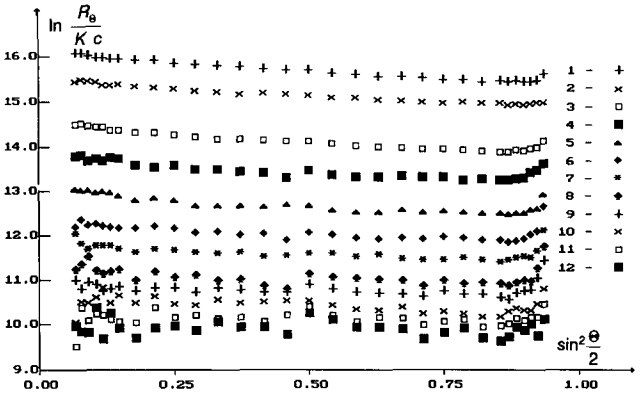

Fig. 9. Guinier plot of selected fractions from Fig. 8. 3, $M_w = 9{\cdot}53 \times 10^6$; 4, $M_w = 5{\cdot}24 \times 10^6$; 5, $M_w = 1{\cdot}94 \times 10^6$; 6, $M_w = 9{\cdot}14 \times 10^5$; 8, $M_w = 4{\cdot}24 \times 10^5$; 10, $M_w = 2{\cdot}02 \times 10^5$; 12, $M_w = 1{\cdot}30 \times 10^5$; 14, $M_w = 7{\cdot}30 \times 10^4$; 16, $M_w = 5{\cdot}20 \times 10^4$; 18, $M_w = 3{\cdot}94 \times 10^6$; 20, $M_w = 2{\cdot}75 \times 10^4$; 22, $M_w = 2{\cdot}21 \times 10^4$.

of pectins as linear polymer homologous series contaminated with some high molecular impurities. Pectins appeared much better represented by an extremely broad molecular weight distribution between a few thousands and hundreds of millions. As the molecular weight increases, so does the average degree of branching by neutral sugar side chains. Correspond-

ingly, species change their conformation from rods (Harding *et al.*, 1991*a*; Berth, 1992) at low molecular weights to compact spheres at the top of the molecular weight distribution. We have explained the variety of architectures at any stage of the distribution on the concept of alternatingly arranged smooth and hairy regions (de Vries *et al.*, 1982) where the size of hairy regions can vary even intramolecularly. The high molecular nature of hairy regions (Schols *et al.*, 1990; Häßlin, 1991) and even their bimodal distribution were confirmed elsewhere (Schols *et al.*, 1990), albeit the pectins chosen in the latter studies as standards for calibrating HPSE led to an underestimate of molecular weights due to the much more compact nature of the hairy regions (Berth, unpublished).

We do not agree with the definition of pectins as 'highly branched species of microgel-like structure independent of their degree of esterification' as was concluded from simultaneous static and dynamic light scattering measurements after filtration through 1·2 μm pore size membrane filters (Häßlin, 1991). This model overemphasizes, according to the theory of light scattering, the largest species within the population and cannot explain the viscosity behaviour of pectins and their Mark–Houwink plots (Pals & Hermans, 1952; Hourdet & Muller, 1987, 1991; Axelos *et al.*, 1989). Sphere-like or microgel-like structures were observed though, even when sharper filtration conditions had been applied (Chapman *et al.*, 1987).

The present contribution strengthens our previous argument that pectins have a broad and overlapping size and density distribution due to their chemical heterogeneity. 'Purification' or clarification under these circumstances cuts off the long high molecular weight dense tail, but still leaves a heterogeneous mixture of strictly individual composition. This makes it possible to understand why general correlationships between the average molecular weight and intrinsic viscosity and gel strength (Säverborn, 1945; Devine, 1974; Smith, 1976) could not be found unless the series is prepared from a single sample by degradation (Berth *et al.*, 1977), esterification (Plashchina *et al.*, 1985; Berth *et al.*, 1982) or GPC. Data from different sample series could never be mixed (Berth & Lexow, 1991).

The problem of association will be the subject of Part III of this series.

ACKNOWLEDGEMENTS

We thank Dr T.P. Kravtchenko (Sanofi, France) for analysing the chemical composition of the pectin samples during his time at the Agricultural University, Wageningen (The Netherlands), and Mrs Evelyn Lück in Potsdam-Rehbrücke for her careful laboratory assistance.

REFERENCES

Axelos, M.A.V., Thibault, J.F. & Lefebre, J. (1989). *Int. J. Biol. Macromol.*, **11**, 186–90.
Berth, G. (1988). *Carbohydr. Polym.*, **8**, 105–18.
Berth, G. (1988). *Carbohydr. Polym.*, **19**, 1–9.
Berth, G. & Dahme, A. (1991). *Food Hydrocoll.*, **5**, 101–4.
Berth, G. & Lexow, D. (1991). *Carbohydr. Polym.*, **15**, 51–66.
Berth, G., Anger, H. & Linow, F. (1977). *Nahrung*, **21**, 939–50.
Berth, G., Anger, H., Plashchina, I.G., Braudo, E.E. & Tolstogusov, V.B. (1982). *Carbohydr. Polym.*, **2**, 1–8.
Berth, G., Dautzenberg, H., Lexow, D. & Rother, G. (1990). *Carbohydr. Polym.*, **12**, 39–59.
Chapman, H.D., Morris, V.J., Selvendran, R.R. & O'Neill, M.A. (1987). *Carbohydr. Res.*, **165**, 53.
Dautzenberg, H. & Rother, G. (1988). *J. Polym Sci., Part B, Polym. Phys.*, **26**, 353–66.
Devine, W.C. (1974). Physico-chemical studies on pectins. PhD Thesis. Univ of Edinburgh, UK.
Harding, S.E., Berth, G., Ball, A., Mitchell, J.R. & de la Torre, G. (1991*a*). *Carbohydr. Polym.*, **16**, 1–15.
Harding, S.E., Vårum, K.M., Stokke, B.T. & Smidsrød, O. (1991*b*) *Advances in Carbohydrate Analysis* Vol. 1, ed. C.A. White. JAI Press, London and Greenwich, pp. 63–144.
Häßlin, B. (1991). Lichtstreuuntersuchungen an Pektinen und bakteriellen Kapselpolysacchariden. PhD Thesis. Albert-Ludwigs-Universität Freiburg im Breisgau, Germany.
Hourdet, D. & Muller, G. (1987). *Carbohydr. Polym.*, **7**, 301–12.
Hourdet, D. & Muller, G. (1991). *Carbohydr. Polym.*, **16**, 409–32.
Huglin, M.B. (ed.) (1972). *Light Scattering from Polymer Solutions*. Academic Press, London, New York.
Kerker, M. (1969). *The Scattering of Light and Other Electromagnetic Radiation*, Academic Press, New York, San Francisco, London.
Kratochvil, P. (1972). In *Light Scattering from Polymer Solutions*, ed. M.B. Huglin. Academic Press, London, New York.
Kravtchenko, T.P., Voragen, V.A.J. & Pilnik, W. (1992). *Carbohydr. Polym.*, **18**, 17.
Pals, D.T.F. & Hermans, J.J. (1952). *Recueil*, **71**, 433.
Plashchina, I.G., Semenova, M.G., Braudo, E.E. & Tolstogusov, V.B. (1985). *Carbohydr. Polym.*, **5**, 159–79.
Säverborn, S. (1945). *A Contribution to the Knowledge of the Acid Polyuronides*, Almquist & Wiksell, Uppsala, Sweden.
Schols, H., Posthumus, M.A. & Boragen, A.G.J. (1990). *Carbohydr. Res.*, **206**, 117–29.
Smith, J.E. (1976). The molecular weights of pectins. PhD Thesis. University of Leeds, UK.
Tanford, C. (1965). *Physical Chemistry of Macromolecules*, John Wiley, New York.
Vries, J. de, Rombouts, F.M., Voragen, A.G.J. & Pilnik, W. (1982). *Carbohydr. Polym.*, **2**, 25–34.
Zimm, B.H. (1948). *J. Chem. Phys.*, **16**, 1099–116.